www.amlett.com, www.vbripress.com/aml, DOI: 10.5185/amlett.2015.5875 Published online by the VBRI Press in 2015

An investigation of electrical, magnetic and optical properties of $La_{1-x}Ca_xMnO_3$ (x= 0.0, 0.3, 0.5 and 0.7) system

Khalid Sultan*, M. Ikram*

Solid State Physics Lab, Department of Physics, National Institute of Technology Hazratbal Srinagar, J & K 190006, India

*Corresponding author. Tel: (+91) 9419031528; E-mail: ksbhat.phy@gmail.com

Received: 28 February 2015, Revised: 18 March 2015 and Accepted: 20 March 2015

ABSTRACT

Results from a detailed investigation on the structural, optical, electrical and magnetic properties of polycrystalline bulk samples of $La_{1-x}Ca_xMnO_3$ (x=0, 0.3, 0.5 and 0.7) synthesized by solid state reaction method are presented. The Rietveld analysis of the X-Ray diffraction (XRD) profiles clearly indicated that the XRD patterns are well fitted with orthorhombic structure. Raman spectral features revealed their finger print modes and irreducible representations at the brillouin zone center as per the group theory. It is also observed that as doping is increased, these compounds tend towards a cubic form. Ooptical band gap 'E_g' study reveals that the Eg decreases with Ca doping resulting in increase in conductivity. This is consistent with the resistivity measurements. In all the samples, except when x = 0.0 and 0.7, the resistivity at the highest temperature measured ($\rho_{300\,K}$) is less than that at 5 K (ρ_{5K}), although for temperature T<Tp, the material shows a metal variation of ρ with temperature (d ρ/dT > 0) whereas the value of $\rho_{300\,K}$ decreases as x increases. Magnetization study revealed that temperatures corresponding to magnetic transitions Tc increases with doping. It is observed that the composition x = 0.5 show both a paramagnetic to ferromagnetic transition and an antiferromagnetic transition. An effort has been made to relate above observed results in the compound with the structural changes brought about by Ca doping. Possible mechanisms such as activated transport and Zener double exchange are used to understand the phase diagram of these materials. Copyright © 2015 VBRI Press.

Keywords: Manganites; magnetization; zener double exchange; activation energy.

Introduction

The mixed valent oxides of the type $R_{1-x}A_xMnO_3$ where R is a rare earth element and A the divalent cation Ca, Sr, or Ba have been a subject of scientific investigations for many decades [**1-4**]. The recent interest in these compounds emanates from the observation of a large negative magnetoresistance [**5, 6**], charge and spin ordering effects as a function of Mn^{3+}/Mn^{4+} ratio [**7-10**] and similarity of many issues with the problem of high Tc superconductivity in the cuprates [**11**]. Effect of doping on various physical properties of the compounds has been widely studied [**12-19**].The rich phase diagram of $La_{1-x}A_xMnO_3$ is a result of interplay between spin, charge, lattice and orbital degrees of freedom [**20**]. The partial substitution of trivalent La by divalent Ca results in hole doping. In the parent compound of $LaMnO_3$, when La is partially substituted by divalent cations such as Ca, Sr etc results in high Colossal Magnetoresistance (CMR). The parent compound, $LaMnO_3$ (Mn^{3+}; t_{2g} 3, e_g 1) is an antiferromagnetic insulator. Divalent substitution for La^{3+}, in the simplest picture, converts Mn^{3+} ions to Mn^{4+}. The latter is not Jahn-Teller active, thus the average MnO_6 distortion decreases with increasing x. The range of this substitution of Ca, Sr or even Ce is limited by the tolerance factor 't' [which is defined as the ratio of the distance between the cation and the oxygen ions and the Mn-O bond length divided by √2].

i.e., $t = d_{R-O}/\sqrt{2}\, d_{Mn-O}$

Only for the Ca doped $LaMnO_3$ the tolerance factor is close to one and the alloy $La_{1-x}Ca_xMnO_3$ (LCMO) can form over the entire concentration range, $0 \leq x \leq 1$ [**2**]. In the compound LCMO, the Mn ions form approximately a cubic lattice with the oxygen ion located nearly at the center of each side and the La or Ca atoms at the body center of each cube. In the nearly cubic symmetry, the five degenerate 3d levels split into t_{2g} (triplet) and e_g (doublet). In the octahedral coordination, e_g states have higher energy than the corresponding t_{2g} states. The hole doped system LCMO is a mixture of trivalent Mn^{3+} and tetravalent Mn^{4+} ions. With this mixed valency of Mn ions in the system, all the t_{2g} orbitals in both trivalent and tetravalent Mn are singly occupied and results in a total spin of 3/2 in the system. The situation is different for the e_g orbitals, in Mn^{4+} ($3d^3$) the e_g orbitals are empty while as in Mn^{3+} ($3d^4$) e_g orbitals are occupied by a single 3d electron. The t_{2g} and e_g orbitals are ferromagnetically correlated via Hund's rule. The intermediate valence character of Mn ions arises from the hoping of e_g electrons [**21, 22**].

The parent compound $LaMnO_3$ is an antiferromagnetic insulator and the divalent doping at La sites results in the phenomena of CMR in the compound $La_{1-x}A_xMnO_3$ for the doping range of $0.2< x < 0.5$ [**3**]. These compounds show a paramagnetic-to-ferromagnetic phase transition accompanied by a sharp drop in resistivity of the compounds. The phenomena of CMR occur in these materials as a consequence of rapid shift of ferromagnetic transition temperature (Tc) to higher temperature region in the presence of magnetic field. For the doping range of $x > 0.5$, the compound is an antiferromagnetic insulator with the ordering of doped charge carriers [**23**]. The half doped ($x = 0.5$) compound belonging to the system LCMO illustrates a complex mixture of low temperature ferromagnetic (FM) and antiferromagnetic (AFM)/charge ordered (CO) phases [**24, 25**]. This half doped compound at the phase boundary exhibits many extra ordinary properties and has been an interest of recent study [**26, 27**]. One purpose of this divalent substitution is to introduce a mixed valency into the system. In the case of $LaMnO_3$ the formal valencies of the atoms are La^{3+} Mn^{3+} $O^{2-}{}_3$ and for $CaMnO_3$, $Ca^{2+}Mn^{4+}O^{2-}{}_3$, so that (La, Ca) MnO_3 should contain both Mn^{3+} and Mn^{4+} ions. The system is thus mixed valent. Introducing a mixed valency profoundly alters the magnetic and electronic properties of the system. For example, $LaMnO_3$ and $CaMnO_3$ are antiferromagnetic insulators at low temperature but $La_{0.7}Ca_{0.3}MnO_3$ is a ferromagnetic metal. Present study focuses on the structural, optical, electrical and magnetic properties of $La_{1-x}Ca_xMnO_3$ (where x=0, 0.3, 0.5 and 0.7) and evaluates the parameters like lattice parameters, optical band gap, activation energy and the electrical and magnetic transition temperatures. An effort has been made to relate the structural distortions caused by the incorporation of Mn ions with other optical and transport properties. The effect of doping on these parameters is discussed. Possible mechanism for their conduction is also discussed.

Experimental

Polycrystalline bulk samples of chemical composition $La_{1-x}Ca_xMnO_3$ (x=0, 0.3, 0.5 and 0.7) were prepared by solid state reaction method. High purity (> 99.9%) precursors of La_2O_3, Mn_2O_3 and $CaCO_3$ taken in the stoichiometry ratio were mixed and preheated at 1000^0C for 12 hours and then calcinated again at 1200^0C for 12 hours. The homogenous powder was reground and pellets of 10 mm in diameter were made by the application of 5 kN force. The resultant pellets were sintered at 1250^0C for 24 hours at a heating rate of 4^0Cmin^{-1} and then cooled to room temperature at a cooling rate of 3^0C min^{-1} in a tubular furnace.

The calcinated material was analyzed by X-ray diffraction (XRD) using Bruker D8 Advance diffractometer (Cu-Kα radiation). The diffraction angle (2θ) range between 20-80^0 was scanned at room temperature. Raman spectra were recorded with a Labram-HR800 micro Raman spectrometer equipped with a Peltier cooled charge-coupled device detector using an Ar excitation source having a wavelength of 488nm. No melting or phase transition was observed in the sample at excitation of Laser power of 10 mW. Bulk samples of LCMO were dissolved in ethanol and irradiated under ultraviolet-visible radiation to see the effect of Ca doping on maximum absorption wavelength and on optical band gap of systems. Rectangular bars (8 x 6mm) of pellets were used for electrical resistivity measurement which was carried out by using four probe techniques in the temperature range 5K - 300K at a step size of 1 deg/min. The temperature dependent magnetic measurements were carried out in the temperature 5K to 300K by using a Quantum design PPMS-VSM magnetometer with sensitivity upto 10^5 emu/g at a field of 500 Oe both in Field cooled (FC) as well as in Zero field cooled (ZFC) condition.

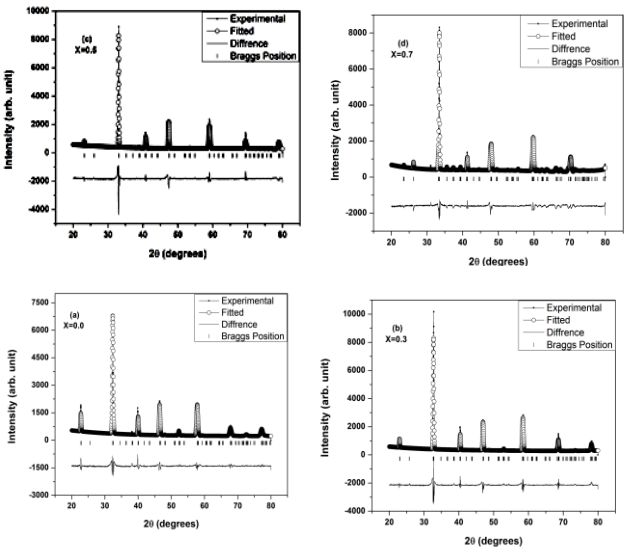

Fig. 1. XRD pattern of $La_{1-x}Ca_xMnO_3$ (x = 0.0, 0.3, 0.5, 0.7). The structure was investigated by Rietveld treatment of the X-Ray diffraction (XRD) profiles.

Table 1. Room temperature lattice parameters, c/a ratio and unit cell volumes of the samples studied in the present work.

Sample	a(Å)	b(Å)	c (Å)	c/a (Å)	Volume (Å^3)
x = 0	5.513	7.773	5.534	1.077	237.17
x = 0.3	5.464	7.723	5.494	1.005	231.83
x = 0.5	5.413	7.672	5.426	1.002	225.33
x = 0.7	5.357	7.568	5.398	1.007	218.84

Results and discussion

XRD analysis

The structure of $La_{1-x}Ca_xMnO_3$ (x=0, 0.3, 0.5 and 0.7) was investigated by Rietveld treatment of the X-Ray diffraction (XRD) profiles recorded with a high- resolution diffractometer and refined parameters were obtained from it. **Fig. 1** shows XRD patterns of LCMO and it clearly indicates that the LCMO are well fitted with orthorhombic structure with space group *Pnma*. In **Table 1** lattice parameters, c/a ratio and the unit cell volume are given which were calculated from the XRD pattern of the samples. It was observed that the lattice parameters, cell volume and c/a ratio monotonically decrease with Ca doping due to change in A-site ionic radius [**28**]. The variation of lattice constants a, b/√2 and c against Ca concentration **(Fig. 2)** clearly shows that with Ca doping,

the lattice parameters change monotonically and the structure starts shifting from orthorhombic to cubic as move from x=0.0 to x=0.7 which is due to increase in Mn^{4+} content in the parent compound $LaMnO_3$ which is consistent with the results obtained by Mahendiran *et al* [**29].**

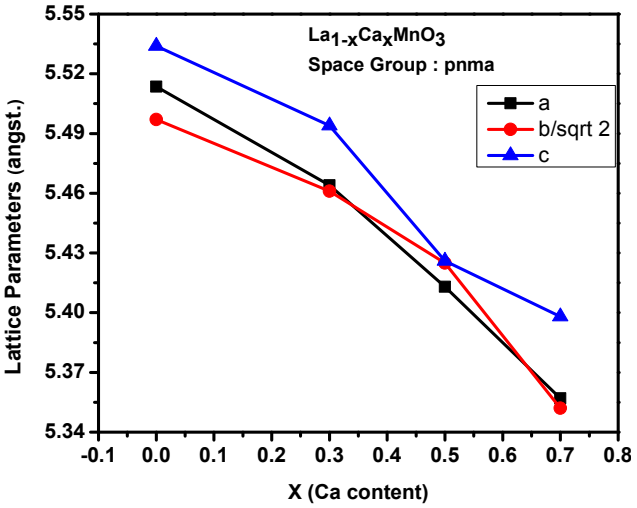

Fig. 2. Variation of lattice constants a, $b/\sqrt{2}$ and c against Ca concentration for the compound $La_{1-x}Ca_xMnO_3$ (x = 0.0, 0.3, 0.5, 0.7).

The cations La and Ca have almost similar size and are randomly substituted on A site. The size of the ions determines the extent of distortion in the compound. If the size of A site cation $r_A < a/\sqrt{2}-r_o$ (here 'a' is the cubic lattice parameter and r_o is the radius of oxygen ion), the distortion will be most probably due to rigid tilts of oxygen octahedron. Whereas on contrarily if $r_B < a/2-r_o$ (r_B is the radius of B site cation) the distortion is most likely due to movement of B site cation within the oxygen octahedron. With these parameters and ionic sizes into consideration it is found that the system in present study follows the former ($r_A < a/\sqrt{2}-r_o$) relation between its contributing ions which suggests that system will most probably be distorted by rotation of oxygen octahedral as is observed at room temperature. This variation has been attributed to the decrease in effective ionic radii of La and Mn on Ca doping. From above discussion it can be concluded that the distortion of MnO_6 octahedra depends not only on the ionic radius of dopant but also depends on the amount of doping.

Raman measurements

Raman signature of perovskite structure arises from the two interpenetrated lattices: the covalent entities constituting the structure (BO_6 octahedron sharing common oxygen ions) and the second one made of highly Columbic ions. These contribute to the translation oscillation modes which couple themselves with other vibrational modes of the neighboring entities: translations and rotations/vibration of iono-covalent BO_6 entity leading to the wave number shifts. The Raman spectra of LCMO compounds at room temperature (300 K) are shown in **Fig. 3** in which it is observed that the B_{2g} mode shifts to higher wave number region with doping. Raman peaks were observed at their finger print positions and are consistent with the literature **[30]**. On account of their high frequency, the Raman features between 450 and 650 cm^{-1} correspond to internal modes **[30-32]**. **Table 2** shows the observed modes with corresponding spectral assignments based on ref. **[33].**

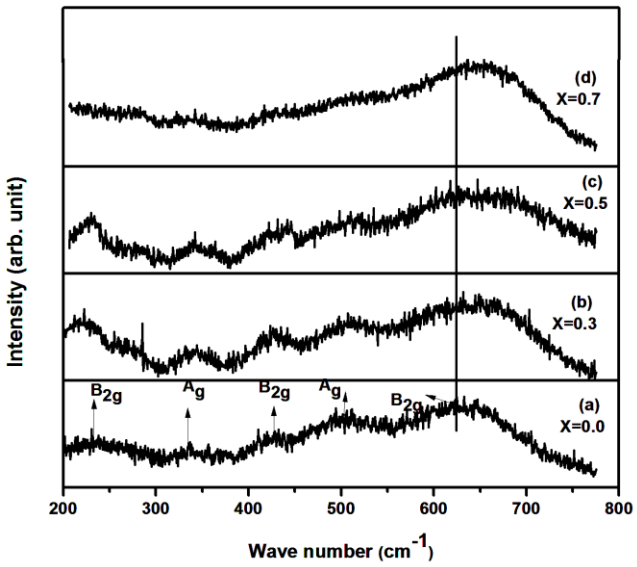

Fig. 3. Raman spectra of $La_{1-x}Ca_xMnO_3$ samples for (a) x = 0.0, (b) x = 0.3, (c) x = 0.5, (d) x = 0.7. Inset shows shifting of B_{2g} mode to higher wave no. region with doping.

Table 2. The observed Raman modes with corresponding assignments.

Symmetry	Present study Mode (cm^{-1})	Main assignment
$B_{2g}(1)$	624	Mn-O, stretching, breathing
$A_g(2)$	499	O-Mn-O, rotation, bending
$B_2g(3)$	427	MnO_6, stretching, rotation
$A_g(4)$	355	MnO_6, stretching, bending
$B_{2g}(5)$	230	MnO_6, bending, breathing

One of the interesting characteristic of Raman scattering is sensitivity towards strain in the sample **[34]**. When the material is under strain, its Raman wave will deform/shift from the original status and in that case mechanical quantity is possible to be measured directly. It is an established fact that the position of the Raman peaks shift towards higher wave number region (Blue shift) due to compressive stress and shift towards lower wave no. (Red shift) due to tensile stress **[35]**. In the present study it is clear from **Fig. 3** that the modes exhibit a blue shift (hardening behavior) with broadening of FWHM's in the doped samples which may arise due to the strain developed in the sample after the inclusion of Ca ions. The observed shift in wave no. with doping clearly indicates in Ca-O/ Mn-O bond lengths as well as impact on MnO_6 octahedra.

The Raman spectra show that there is a disorder in the vibrational bands with increasing Mn content, which is primarily obvious because most of the Raman modes below 600 cm^{-1} are suppressed by the substitution of Ca ions and the only mode visible throughout the series is the B_{2g} (near 624 cm^{-1} in pristine sample). From the above discussion, it is evident that the substitution of Ca ions in $LaMnO_3$ apart from weakening the exchange interaction also induces a J-T distortion which results in a large electric field gradient at the Mn nucleus. The crystallographic structure of the

compound $LaMnO_3$ is modified by the substitution of Ca ions, because the ionic radii of Ca^{2+} and Mn^{3+} in LCMO are different. Hence the double exchange interaction between two Mn ions via the intervening oxygen atom takes place.

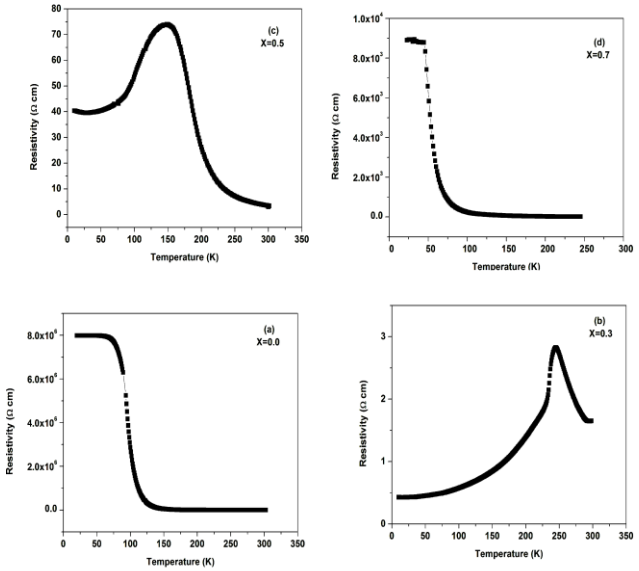

Fig. 4. Temperature dependence of resistivity of polycrystalline pellets of $La_{1-x}Ca_xMnO_3$ samples for (a) x = 0.0, (b) x = 0.3, (c) x = 0.5 and (d) x = 0.7.

Table 3. The values of various calculated parameters such as Tp (Tp is the temperature corresponding to the resistivity peak), *Tc (*Tc is the ferromagnetic curie temperature), activation energy E_a and optical band gap E_g for different compositions of $La_{1-x}Ca_xMnO_3$ (x = 0.0, 0.3, 0.5, 0.7) are summarized.

Composition	Tc(K)	Tp (K)	Ea (eV)	E_g(eV)
X = 0.0	180	*	0.19	1.32
X = 0.3	250	245	0.14	1.14
X = 0.5	255	150	0.12	0.91
X = 0.7	260	*	0.07	0.55

*No peak but a sharp transition.

Optical study

The optical band gap "E_g**"** was calculated from the curve between $(\alpha.\ h\nu)^{1/2}$ and E (eV) where α is the absorption coefficient and E is energy in electron volts (figure not shown). Optical transitions provide direct access to the energy level structure of a system. The compositional values of $\mathbf{E_g}$ are shown in **Table 3**. The calculated values of $\mathbf{E_g}$ are 1.32, 1.14, 0.91 and 0.55 eV for x=0.0, x=0.3, x=0.5 and x=0.7 respectively in the compound $La_{1-x}Ca_xMnO_3$. Red shift with Ca doping concentration is evident from the table III. The JT distortion could be one of the reasons for this observation. In addition, Ca occupies the La site, thus leading to the change of bond angle and bond length. The calculated values of optical band gap "E_g" and variation thereafter with Ca doping is consistent with earlier reports **[29]**. It is clear from our results that the optical band gap decreases with increase in Ca doping resulting in increase in conductivity with Ca doping. Substitution of the Ca ion effectively causes the increase in the density of states which results in decrease of band gap. The decrease in the gap parameter can also indicate that the correlation length in the conducting network is increasing. Hence the optical results are consistent with other transport results (as discussed in next section).

Electrical measurements

The electrical resistivity (ρ) of the samples as a function of temperature **(Fig. 4)** shows that For *T* > Tp (Tp is the temperature corresponding to the resistivity peak), the resistivity shows activated transport as in an insulator. Activation energy (E_a**)** was calculated from the slope of the curve log ρ vs. 1000/T (K^{-1}) using relation $\rho = \rho_0 e^{-Ea/kT}$ and was found to be in the range of 0.19 to 0.07 eV (**Table 3**). Here ρ_0 is the conductivity at infinite temperature and k is the Boltzmann's constant and *Ea* is the activation energy. The prefactor ρ_0 is of the order of 1.5 mΩ implying that the holes are localized in the paramagnetic phase most probably due to coulomb attraction of the divalent cation, or lattice distortion around it. The value of E_a in the paramagnetic regime decreases progressively as x increases **(Table 3).**

At T=300 K, all compositions are classed as paramagnetic insulators and have an orthorhombic crystal structure **[36]**. The samples show general behavior of decrease in resistivity with Ca doping which cannot simply be due to the changes in disorder of the La and Ca ions as the composition is changed (resistivity would peak at *x* = 0.5) nor can be explained solely by the number of free carriers in the system otherwise the resistivity would be minimal at *x* = 0.5 where the number of Mn^{3+} ions with itinerant electrons is equal to the number of Mn^{4+} ions. The most likely explanation is that it is due to changes in the crystal structure that occur as the calcium doping is changed. It is also evident from **Fig. 2** that as doping is increased, the material tends towards a cubic form, as is evident from change in lattice parameters. It is a general result that closer to cubicity a sample is, the lower is its resistivity. For example, when manganite samples are cooled below their insulator to metal transition temperature, they also become more cubic **[26]**. The effect is also seen in first principle calculations of electronic structure in which simulations with a cubic structure are often metallic but those where the manganite has the same composition but an orthorhombic structure give rise to a band gap. The data from Miller *et al.* **[37]** shows a sharp increase in the resistivity for both end members: $LaMnO_3$ and $CaMnO_3$. This is reminiscent of the large change in resistivity observed in semiconducting materials when donor or acceptor levels are introduced by doping with small quantities of atoms with a different valency. It is likely that the $LaMnO_3$ sample used in this investigation contains an excess of oxygen which introduces a mixed valency into the system (sometimes this process is referred to as 'self-doping') which could reduce the resistivity by orders of magnitude.

For the composition X = 0.5, the resistivity at the highest temperature measured (ρ_{300K}) is less than that at 5 K ($\rho_{5\ K}$), although for T< Tp, the material shows a metal-like variation of resistivity with temperature (d ρ/dT > 0). The reported results were in good agreement with the literature **[28]**. The resistivity at lowest measured temperature is ~ 40

Ωcm which is very high compared to the typical Mott resistivity (ρ_{Mott}) which may be due to the grain boundaries **[38]**. The end members show a high resistivity comparable with the charge ordered compounds, even though they are not charge ordered because only one Mn valency is present. The sharp increase in resistivity for end members of the series is possibliy due to large change in resistivity observed in semiconducting materials when acceptor or donor levels are introduced by doping with small quantities of atoms with a different valence.

The main feature of **Fig. 4** plots is that the resistivity changes by some orders of magnitude between x = 0.3 and x = 0.5. Compounds with x < 0.5 are referred to as metallic and those more resistive samples with x > 0.5, are thought to be in a charge ordered insulating state where ions of different valence localize at specific locations within the crystal, leading to the dramatic rise in resistivity. The room temperature resistivity gives no indication of phase transition (**Fig. 4)** whereas resistivity shows peak for x = 0.5 and then fall with increasing doping.

Magnetic measurements

The zero-field-cooled (ZFC) and field-cooled (FC) magnetization as a function of temperature at 500 Oe field are shown in **Fig. 5**. The sample shows irreversible behavior with closed loops of ZFC and FC curves. The large difference between *M*FC and *M*ZFC at low temperatures suggests an inhomogeneous mixture of a ferromagnetic and antiferromagnetic rather than a distinct ferromagnetic or antiferromagnetic long range order. It is seen from the **Table 3.** (temperature corresponding to magnetic transitions "Tc") that Tc increases with increase in doping. The parent compound $LaMnO_3$ is an antiferromagnetic insulator and the divalent doping at La sites results in the phenomena of CMR for the doping range of 0.2< x < 0.5 due to rapid shift of ferromagnetic transition temperature (Tc) to higher temperature region in the presence of magnetic field. For the doping range of x = 0.7, the compound is an antiferromagnetic insulator with the ordering of doped charge carriers. The compound $La_{0.5}Ca_{0.5}MnO_3$ shows coexistence of two totally dissimilar ground states i.e., ferromagnetic-metallic and antiferromagnetic-charge ordered which is also consistent with the earlier reports **[39, 40]**.

A qualitative picture of the behavior displayed by the mixed valent manganite $La_{0.5}Ca_{0.5}MnO_3$ can be attributed to the concept of Zener double exchange **[41]**. Actually it revolves around the changing valency of Mn from $Mn^{4+} \leftrightarrow Mn^{3+}$ i,e there is hopping of a 3d hole from Mn^{4+} (d^3, $T_{2g}(3)$, S=3/2), to Mn^{3+} (d^4, $T_{2g}(3)$, e_g (1), S=2), *via* the intervening ligand oxygen. Electrons are thought to hop between neighboring Mn ions via the intervening oxygen atom. During hopping spin of electrons will be preserved provided some scattering doesn't take place during transfer of electrons. The ferromagnetic alignment is energetically favorable as Hund's rule coupling makes it favorable for the spin of electrons to align with the spin of the itinerant electrons. This hopping of electrons between Mn ions is also responsible for conductivity in the compound. The oxygen between Mn ions is regarded as having a passive role in the conduction process. The spins of every Mn ion is aligned parallel in ferromagnetic phase so has the best conductivity whereas antiferromagnetic phase having the antiparallel arrangement of spins have the least conductivity, while as the conductivity of paramagnetic phase is intermediate. Based on this zener double exchange a paramagnetic to ferromagnetic transition occurs in the compound.

It is clear from **Fig. 5** that the compound with composition x = 0.5 shows both a paramagnetic to ferromagnetic transition at around 250 K and then an antiferromagnetic transition at around 170 K. The large hysteresis is reported in literature for these compounds **[42, 43]**. This observed hysteresis proves to be an indication that charge ordering is a nucleation and growth process. The compound $La_{0.5}Ca_{0.5}MnO_3$ illustrates a complex mixture of low temperature ferromagnetic and antiferromagnetic /charge ordered phases. At temperatures well below the Neel temperature, the magnetization for the compound is still higher possibly due to spin canting **[26, 44]** or an inhomogeneous mixture of ferromagnetic and antiferromagnetic regions within the compound.

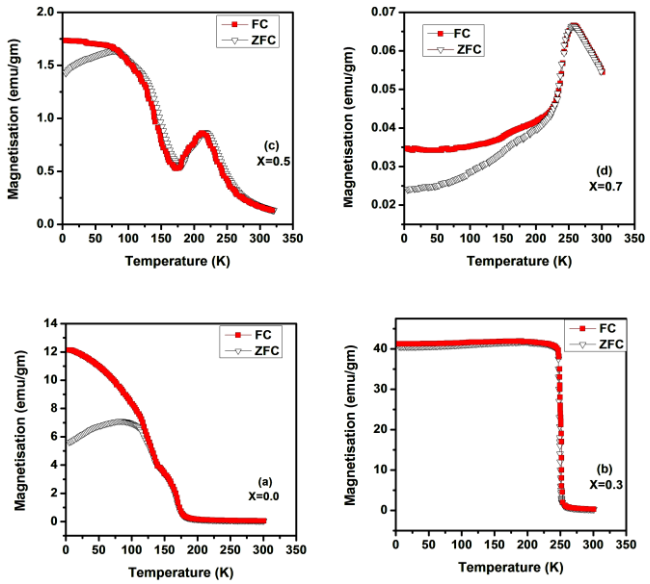

Fig. 5. Temperature dependence of zero-field cooled and field cooled magnetization plots (in the presence of 500 Oe magnetic field) for polycrystalline pellets of $La_{1-x}Ca_xMnO_3$ samples for (a) x = 0.0, (b) x = 0.3, (c) x = 0.5 and (d) x = 0.7.

The Ca doped LCMOs exhibit three basic phases: insulating paramagnetic, ferromagnetic with metallic-like conductivity and charge-ordered antiferromagnetic insulating phases. In this doping range it is possible to have multiple phases coexisting. The experimental results were somewhat unfavorable due to presence of various defects such as dislocations and grain boundaries occurred during the synthesis and measurement process. These defects caused the slight change in balancing the competing phases, hence creating the nucleation sites, and existence of extrinsic phase separation. At low doping the single stripe within a charge ordered region is quite minute and cannot be considered as disconnected phase which limits to the extension of phase. There are also considerations which limits the spatial extent of a phase. For example, a single stripe within a charge ordered region is too small to be a separate thermodynamic entity and cannot be considered as

a separate phase. Transition is observed from PM phase to FM at temperature T = T_C, where T_C is a Curie temperature. Similarly at this temperature metal-insulation (M-I) transition is observed in LCMO, enhancing the metallic behavior, where T = T_C = TMI and the PMI phase observed in high temperature turns into ferromagnetic metallic (FMM) state, hence leading to the extraction of metallic like conductivity in the FM phase. With further fall in temperature FM bunches and clusters are produced, increasing the percolation path. In case of T > TC, LCMO is usually a paramagnetic insulator (PMI) in which the electron hopping mechanism through dielectric insulators generates electrical conductivity. The main three mechanisms involved in the conduction phenomenon with experimental confirmation are, thermally activated hopping model **[45]**, the nearest neighbors hopping model [46] and a variable range hopping (VRH) model **[47]**. The synthesis process and their measurement is carried out in very confined temperature range i.e. just above Tc, which prevents to make distinction between the three mechanism, consequently, there is no agreement as to which mechanism actually prevails **[48-49]**.

The M–H plots at T = 5K and 300 K for Ca doped $LaMnO_3$samples are shown in **Fig. 6(a)** and **Fig. 6(b)** respectively. The appearance of ferromagnetism in these samples at low temperature (5 K) upto to doping concentration of x = 0.5 may be attributed to the canting of the antiferromagnetically ordered spins by the structural distortion. But at x=0.7, the material shows paramagnetic behavior as it is showing the linear behavior with magnetic field. Also a remarkable change occurs at 300 K, where the magnetization shows linear behavior with magnetic field, indicating that the overall magnetic behavior is paramagnetic type. The dramatic change in the magnetization curves shows that, at higher temperature, the paramagnetic behavior of La sublattices dominates over the system. During double exchange interaction two neighboring manganese atoms and their connecting oxygen atom play a role. One of the manganese atoms has one of it's e_g states occupied, the other has an empty e_g shell. One electron tunnels from the oxygen atom to the manganese atom without eg electrons. The e_g electron from the other manganese atom then tunnels to the freed 2p position on the oxygen atom. The net result is one electron moving from one manganese atom to the next. The qualitative picture of the behavior displayed by the mixed valent manganite $La_{0.5}Ca_{0.5}MnO_3$ is attributed to the concept of Zener double exchange.

From the structural analysis of LCMO compounds, the bond length decreases with Ca substitution whereas Mn-O-Mn bond angle also increases from 153° in orthorhombic (x = 0.0) to about 180° in cubic samples. With increasing Mn^{4+} in the compound (i.e. with increasing Ca doping) the r_{M-O} bond length decreases because of a comparatively a greater overlap between metal and oxygen orbitals which might also result in decrease in optical band gap (table III). Because of the change in bond length of r_{M-O} and consequent change in bond angle of Mn-O-Mn , the $B_{2g}(1)$ peak in Raman spectra ($624cm^{-1}$) which is due to Mn-O, stretching-breathing develops strain and the mode gets shifted towards higher wave no. regions **(Fig. 3)**. The transport properties also highly depend on the structural changes caused by Ca doping.

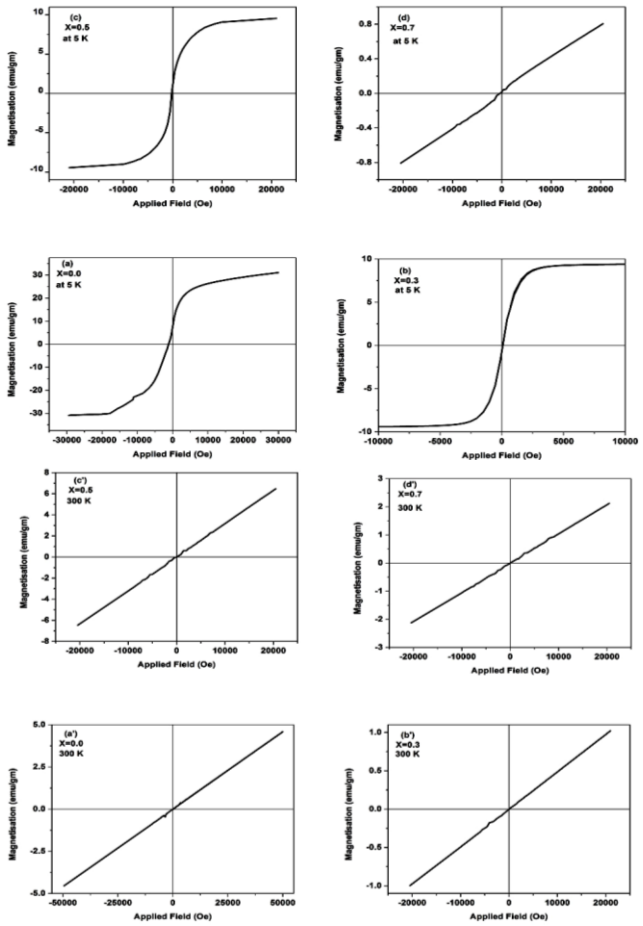

Fig. 6. Magnetization vs field curves for $La_{1-x}Ca_xMnO_3$ samples at 5 K for (a) x = 0.0, (b) x = 0.3, (c) x = 0.5, (d) x = 0.7 and 300 K (a') x = 0.0, (b') x = 0.3, (c') x = 0.5 and (d') x = 0.7.

Conclusion

Ca doped $LaMnO_3$ compounds were synthesized by solid state reaction technique. The substitution of Ca for La ions at A-site results in significant changes in the physical properties of compound. Optical band gap of the compound was also observed to decrease with Ca doping resulting in increase in conductivity in the compound. From resistivity measurements, it is seen that for $T > Tc$, the resistivity shows activated transport and such behavior is similar to insulator. The calculated activation energy (E_a**)** was found to be in the range of 0.19 to 0.07 eV. The compounds show a general decrease in resistivity with Ca doping. For the composition x = 0.5, the compound showed metal like behavior for temperature T < Tp. From the magnetic measurements it was seen that the samples show irreversible behavior with closed loops of ZFC and FC curves. The large difference between *M*FC and *M*ZFC at low temperatures suggests an inhomogeneous mixture of a ferromagnetic and antiferromagnetic rather than a distinct ferromagnetic or antiferromagnetic long range order. The bond length decreases with Ca substitution whereas Mn-O-Mn bond angle increases from 153° in orthorhombic (x = 0.0) to about 180° (x = 0.7). The qualitative picture of the

behavior displayed by the mixed valent manganite $La_{0.5}Ca_{0.5}MnO_3$ was attributed to the concept of Zener double exchange.

Acknowledgements

Authors (K.S and M.I) thank Dr. Alok Banerjee, Dr. R. Rawat IUC, CSR Indore for the magnetic and transport measurements respectively. Authors would also like to thank Director IUAC, New Delhi for necessary experimental facilities and Director NIT Srinagar for encouragement provided during work.

Reference

1. Jonker, G. H.; van Santen, J. H.; *Physica Amsterdam* **1950,** *16*, 337. **DOI:** 10.1016/0031-8914(50)90033-4
2. Wollan, E.O.; Koehler, W.C.; *Phys. Rev*.**1951,** *100*, 545. **DOI:** 10.1103/PhysRev.100.545
3. Bhagat, S.; Amar Nath, K.; Chandra, K.P.; Singh, R.K.; Kulkarni, A.R.; Prasad. K.; *Adv. Mat. Lett*. **2014**, *5(3)*, 117 **DOI:** 10.5185/amlett.2013.fdm.28
4. Suresh,P.; Srinath. S.; *Adv. Mat. Lett*. **2014**, *5(3)*, 127. **DOI:** 10.5185/amlett.2013.fdm.34
5. Von Helmolt, R.; Wecker, J.; Holzapfel, B.; Schultz, L.; Samwer, K.; *Phys. Rev. Lett.* **1993,** *71***,** 2331. **DOI:** 10.1103/PhysRevLett.71.2331
6. Jin, S.; Mc Cormack, M.; Tiefel, T.H.; Ramesh, R.; *J. Appl. Phys*. **1994,** *76***,** 6929. **DOI:** 10.1063/1.358119.
7. Yoshizawa, H.; Kawano, H.; Tomioka, T.; Tokura, Y.; *Phys. Rev.*; 1995**,** *52***,** 13145. **DOI:** 10.1103/PhysRevB.52.R13145.
8. Goodenough, J.B.; Phys. Rev. **1967,** *164*, 785. **DOI:** 10.1103/PhysRev.164.785
9. Gaikwad, V.M.; Acharya, S.A.; *Adv. Mat. Lett*. **2014**, *5(3)*, 157 **DOI:** 10.5185/amlett.2013.fdm.82
10. Rani,R.; Juneja, J.K.; Singh,S.; Raina, K.K.; Prakash, C.; *Adv. Mat. Lett*. **2014**, *5(4)*, 229. **DOI:** 10.5185/amlett.2013.fdm.63
11. Khomskii, D.I.; Sawatzky, G.A.; *Solid State Commun*. **1997,** *102*, 87. **DOI:** 10.1016/S0038-1098(96)00717-X
12. Kumar, V.; Bedyal, A.K.; Sharma, J.; Kumar, V.; Ntwaeaborwa, O. M.; Swart. H. C.; *Appl. Phys. A*, **2014**, *116*, 1785. **DOI:** 10.1007/s00339-014-8331-5.
13. Kumar, V.; Kumar, V.; Som, S.; Duvenhage, M.M.; Ntwaeaborwa, O.M.; Swart, H.C.; *Appl. Surf. Sci.*, **2014**, *308*, 419. **DOI:** 10.1016/j.apsusc.2014.04.192
14. Prestgard, M.C.; Siegel, G. P.; Tiwari, A.; *Adv. Mat. Lett*. **2014**, *5(5)*, 242. **DOI:** 10.5185/amlett.2014.amwc1032
15. Chandra, U.; Asokan, K.; Ganesan. V.; *Adv. Mat. Lett*. **2013**, *4(11)*, 862. **DOI:** 10.5185/amlett.2013.4455
16. Sultan, K.; Ikram, M.; Gautam,S.; Lee, H.K.; Chae, K.H.; Asokan. K.; *J. Alloys Compounds*, **2015**, 628, *152*. **DOI:** 10.1016/j.jallcom.2014.11.196.
17. Som, S.; Kunti, A.K.; Kumar, A.K.; Kumar,V.; Dutta, S.; Chowdhury M.;, Sharma, S.K.; Terblans, J.J.; Swart, H.C.; *J. Appl. Phys*. **2014,** *115*, 193101. **DOI:** 10.1063/1.4876316
18. Cao,Y.; Gang Ai, S.; Zhang, J.; Gu, N.; Hu. S.; *Adv. Mat. Lett.* **2013**, *4(2)*, 160. **DOI:** 10.5185/amlett.2012.6366
19. Rai,R.; Coondoo, I.; Valente, M. A.; Kholkin.A.L; *Adv. Mat. Lett*. **2013**, *4(5)*, 354. **DOI:** 10.5185/amlett.2012.9428
20. Salamon, M.B.; Jaime, M.; *Rev. Mod. Phys*. **2001,** *73*, 583. **DOI:** 10.1103/RevModPhys.73.583
21. Schlottmann, P.; *Phys. Rev. B*, **2008**, *77*, 104446. **DOI:** 10.1103/PhysRevB.77.104446
22. Goodenough,; *J. Phys. Rev.* **1955,** *100*, 564. **DOI:** 10.1103/PhysRev.164.785.
23. Schiffer, P.; Ramirez, A.P.; Bao, W.; Cheong, S.W.; *Phys. Rev. Lett.* **1995,** *75*, 3336. **DOI:** 10.1103/PhysRevLett.75.3336
24. Mori, S..; Chen, C.H.; Cheong, S..; *Phys. Rev. Lett.* **1998,** *81*, 3972. **DOI:** 10.1103/PhysRevLett.81.3972
25. Tomioka, Y..; Asamitsu, A..; Moritomo, Y..; Kuwahara, H..; Tokura, Y..; *Phys. Rev. Lett*. **1995,** *74*, 5108. **DOI:** 10.1103/PhysRevLett.74.5108
26. Radaelli, P.G.; Cox, D.E.; Marezio, M.; Cheong, S.W.; Schiffer, P.E.; Ramirez, A.P.; *Phys. Rev. Lett*. **1995**, *75*, 4488. **DOI:** 10.1103/PhysRevLett.75.4488.
27. Singh, M.; Kumar, M.; Štěpánek, F.; PUlbrich, P.; Svoboda, E. Santava, M.; Singla, L.; *Adv. Mat. Lett*. **2011,** 2, 409. **DOI:** 10.5185/amlett.2011.4257
28. Samancloglu, Y.; Coskun, A.; *J. Alloys Compd*. **2010,** *507*, 385. **DOI:** 10.1016/j.jallcom.2010.07.212.
29. Mahendiran, R.; *Phys. Rev. B*. **1996,** *53*, 6. **DOI:** 10.1103/PhysRevB.53.12160
30. Yoon, S.; Ru¨bhausen, M.; Cooper, S.L.; Kim, K.H.; Cheong, S.W.; *Phys. Rev. Lett*. **2000,** *85*, 3297. **DOI:** 10.1103/PhysRevLett.85.3297.
31. Yamamoto, K.; Kimura, T.; Ishikawa, T.; Katsufuji, T.; Tokura, Y.; *Phys. Rev. B*. **2000,** *61*, 14706. **DOI:** 10.1103/PhysRevB.61.14706.
32. Argiriou, D.N.; Bordallo, H.N'; Campbell, B.J.; Cheetham, A.K.; Cox, D.E.; Gardner, J.S.; Hanif, K.; Santos, A.D.; Strouse, G.F.; *Phys. Rev. B.* **2000,** *61*, 15269. **DOI:** 10.1103/PhysRevB.61.15269.
33. Singh, K.M.; Jang, M.H.; Gupta, H.C.; Katiyar, S.R.; *J. Raman Spectrosc.* **2008**, *39*, 842. **DOI:** 10.1002/jrs.1923.
34. Anastassakis, E.; Canterero, A.; Cardona, M.; *Phys. Rev. B***,** **1990,** *41*, 7529. **DOI:** 10.1103/PhysRevB.41.7529.
35. Campbell, I.H.; Fauchet, P. M.; *Solid State Comm.* **1986,** *58***,** 739. **DOI:** 10.1016/0038-1098(86)90513-2.
36. Cheong S.-W.; Hwang H.Y. 'Ferromagnetism vs. Charge/Orbital Ordering' in Ch. 7 *Colossal Magnetoresistive Oxides – Monographs in Condensed Matter Science*. (ed. Tokura Y.), Monogr. In Condensed Matter Sci, Gordon & Breach, Reading, **2000**.
37. Miller, R.C.; Heikes, R.R.; Mazelsky, R.; *J. Appl. Phys.* **1961**, *32***,** 3302. **DOI:** 10.1063/1.1777043
38. Edwards, P. P.; Sienko, M.J.; *Phys. Rev. B.* **1978**, *17*, 2575. **DOI:** 10.1103/PhysRevB.17.2575
39. Moreo, A.; Yunoki, S.; Dagotto, E.; *Science*, **1999**, *283*, 2034. **DOI**: 10.1126/science.283.5410.2034
40. Mathur, N.D.; Littlewood, P.B.; *Sol. Stat. Comm.*, **2001**, *119*, 271. **DOI:** 10.1016/S0038-1098(01)00112-0
41. Zener, C.; Phys. Rev., **1951**, *82*, 403. **DOI**: 10.1103/PhysRev.82.403
42. Uehara, M.; Mori, S.; Chen, C.H.; Cheong, S.W.; *Nature*, **1999,** *399*, 560. **DOI:** 10.1038/21142
43. Levy, P.; *Phys. Rev. B.*, **2000**, *62*, 6437. **DOI:** 10.1103/PhysRevB.62.6437
44. Roy, M.; Mitchell, J.F.; Ramirez, A.P.; Schiffer, P.; *Phys. Rev. B.*, **1998**, 58, 5185. **DOI:** 10.1103/PhysRevB.58.5185
45. Kusters, R. M.; Singleton, J.; Keen, D.A.; McGreevy, R.; Hayes, W.; *Physica B* **1989,** *155*, 362. **DOI:** 10.1016/0921-4526(89)90530-9
46. Snyder, G.J.; Hiskes, R.; DiCarolis, S.; Beasley, M. R.; Geballe, T. H.; *Phys. Rev. B* 53,**1996**, *62*, 14434. **DOI:** 10.1103/PhysRevB.53.14434
47. Viret, M.; Ranno, L.; Coey, J.M.D.; *Phys. Rev. B* .**1997**, 55, 8067. **DOI:** 10.1103/PhysRevB.55.8067
48. Sultan,K.; Ikram, M.; Asokan, K.; *J. Vaccum* **2013**. **DOI:** 10.1016/j.vacuum.2013.06.014.
49. Sultan,K.; Habib,Z.; Jan,A.; Mir, S.A.; Ikram, M.; Asokan, K.; *Adv. Mat. Lett*. **2014**, *5(1)*, 9. **DOI:** 10.5185/amlett.2013.6496

